



# Ta–O–C chemical bond enhancing charge separation between Ta<sup>4+</sup> doped Ta<sub>2</sub>O<sub>5</sub> quantum dots and cotton-like g-C<sub>3</sub>N<sub>4</sub>



Xin Yu<sup>a,b</sup>, Zhonghua Li<sup>b,\*</sup>, Jiawen Liu<sup>c,\*</sup>, Pingan Hu<sup>b</sup>

<sup>a</sup> School of Chemistry and Chemical Engineering, Harbin Institute of Technology, Harbin 150001, PR China

<sup>b</sup> Key Laboratory of Microsystems and Microstructures Manufacturing, Ministry of Education, Harbin Institute of Technology, Harbin 150001, PR China

<sup>c</sup> Key Laboratory for Photonic and Electronic Bandgap Materials, Ministry of Education, Harbin Normal University, Harbin 150025, PR China

## ARTICLE INFO

### Article history:

Received 18 September 2016

Received in revised form 1 December 2016

Accepted 15 December 2016

Available online 15 December 2016

### Keywords:

Self-doped Ta<sub>2</sub>O<sub>5</sub> quantum dots

Cotton-like g-C<sub>3</sub>N<sub>4</sub>

Charge separation

Visible light photocatalysis

Hydrogen production and RhB degradation

## ABSTRACT

We successfully synthesized a novel Ta<sup>4+</sup> self-doped Ta<sub>2</sub>O<sub>5</sub> quantum dots and the self-doped Ta<sub>2</sub>O<sub>5</sub> quantum dots modified cotton-like g-C<sub>3</sub>N<sub>4</sub> nanosheet (TCN) by vapor hydrolysis reaction and calcining treatment. The as-prepared Ta<sub>2</sub>O<sub>5</sub> showed excellent visible light response from 400 to 800 nm, mainly because the formation of Ta<sup>4+</sup> species, which was confirmed by EPR and XPS technology. The estimated bandgap of the self-doped Ta<sub>2</sub>O<sub>5</sub> was ~2.78 eV, which was much lower than that of the commercial Ta<sub>2</sub>O<sub>5</sub> (~4.0 eV), and the visible light photocatalytic activity of the self-doped Ta<sub>2</sub>O<sub>5</sub> for hydrogen production was about 7.98 μmol g<sup>-1</sup> h<sup>-1</sup>. The photocatalytic activity of TCN photocatalyst for hydrogen production and RhB degradation was highly enhanced under visible light irradiation compared with those of g-C<sub>3</sub>N<sub>4</sub> and the self-doped Ta<sub>2</sub>O<sub>5</sub>, indicating the higher charge separation efficiency, which was further confirmed by the photocurrent transient response, electrochemical impedance spectra and PL emission spectra. And the hydrogen evolution rate and the degradation rate constant for RhB degradation of TCN photocatalyst could reach 624.99 μmol g<sup>-1</sup> h<sup>-1</sup> and 0.1512 min<sup>-1</sup>, which were about 3.7 and 11.9 times higher than those of pure g-C<sub>3</sub>N<sub>4</sub>, and 78.29 and 283.78 times higher than those of the self-doped Ta<sub>2</sub>O<sub>5</sub>, much higher than those of the simple physical mixture. The active species trapping experiment of TCN photocatalyst showed that RhB degradation was mainly attributed to the direct hole oxidation. Besides, the XPS results further confirmed that Ta–O–C chemical bond was formed between the as-prepared Ta<sub>2</sub>O<sub>5</sub> and cotton-like g-C<sub>3</sub>N<sub>4</sub>. It was the strong synergistic interactions of Ta–O–C chemical bond and Ta<sup>4+</sup> defect energy level that highly enhanced the photocatalytic activities of TCN catalyst for the hydrogen production and RhB degradation.

© 2016 Elsevier B.V. All rights reserved.

## 1. Introduction

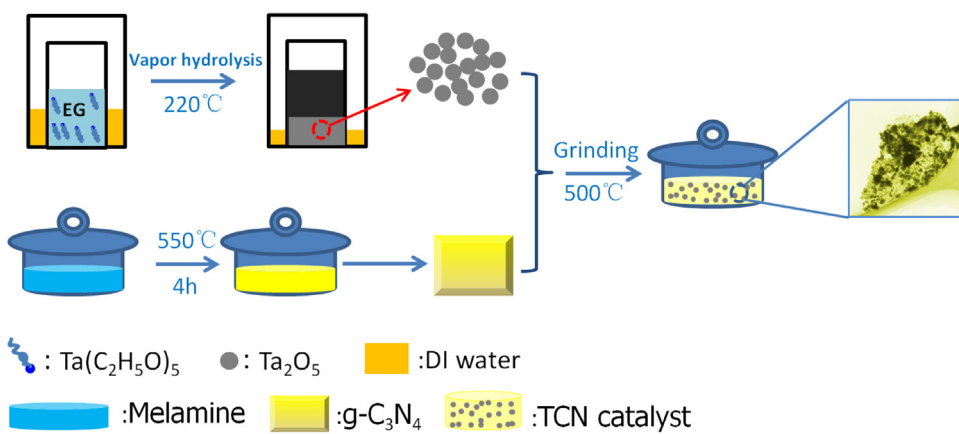
Recently, more attentions have been attracted on the charge separation of the semiconductor photocatalyst for solar energy conversion and pollutant degradation since Fujishima and Honda first discovered that water could be decomposed into hydrogen and oxygen in 1972 [1]. And it is indeed a profitable and promising attempt to relieve the energy crisis and environmental pollution using photocatalysis technology [2–4]. In general, semiconductor is expected to highly accelerate the rate of photocatalytic reaction for solar energy conversion and pollutant degradation [5,6]. However, unlike the nature enzyme catalysts, artificial photocatalysts always suffer from some disadvantages, such as the low charge separa-

tion efficiency, inefficient photocatalytic activity, limited spectral response range and poor photocatalysis stability [7,8]. And therefore, it is urgent for researchers to put insights into the studies of photocatalytic mechanisms by the theoretical calculation and exploit new types of photocatalysts to enhance the charge separation efficiency and extend the spectral response range [9,10]. Until now, fabricating heterojunction photocatalyst is still an effective strategy, which benefits the wide bandgap semiconductors with intriguing visible light response.

Tantalic oxide (Ta<sub>2</sub>O<sub>5</sub>), a typical wide bandgap semiconductor, is a potential and promising photocatalyst in photocatalytic water splitting and pollutant removal. The valence band and conduction band of Ta<sub>2</sub>O<sub>5</sub> were reported to be about -0.17 and +3.83 eV [11], respectively. Thus, it is of great difficulty for wide bandgap Ta<sub>2</sub>O<sub>5</sub> to have visible light photocatalytic activity because of its wide bandgap (~4.0 eV) [12]. Consequently, it is a highly desirable attempt to explore novel Ta<sub>2</sub>O<sub>5</sub> catalysts with visible light response.

\* Corresponding authors.

E-mail addresses: [lizh@hit.edu.cn](mailto:lizh@hit.edu.cn) (Z. Li), [jiawen86@163.com](mailto:jiawen86@163.com) (J. Liu).



**Scheme 1.** Schematic illustration of the formation of the self-doped  $\text{Ta}_2\text{O}_5$  quantum dots and TCN catalysts.

Besides, some researches performed by Xu et al. [13] and Wang et al. [14] showed that fabricating novel heterojunction photocatalyst could contribute to enhance the charge separation and extend the spectral response range. And the novel self-doped  $\text{Ta}_2\text{O}_5$  might also have efficient charge separation efficiency and wide spectral response range.

Graphite carbon nitride ( $\text{g-C}_3\text{N}_4$ ), a novel type of metal-free visible-light semiconductor catalyst, could be obtained from different precursors, including melamine, urea, thiourea, etc [15–17]. Until now,  $\text{g-C}_3\text{N}_4$  has been applied for  $\text{CO}_2$  reduction [18], pollutant removal [19], and hydrogen production from water decomposition [20], mainly because of its suitable electronic structure [21,22]. However, the photocatalytic activities of  $\text{g-C}_3\text{N}_4$  prepared by the traditional methods are not very high because of its lower specific surface area and more defects [23,24]. Some researches on modifying  $\text{g-C}_3\text{N}_4$  have been performed to enhance the photocatalytic activities, such as  $\text{Bi}/\text{g-C}_3\text{N}_4$  [25],  $\text{Au}/\text{Pt}/\text{g-C}_3\text{N}_4$  [26],  $\text{CeO}_2/\text{g-C}_3\text{N}_4$  [27],  $\text{AgX}/\text{g-C}_3\text{N}_4$  [28], etc. The photocatalytic activities of these  $\text{g-C}_3\text{N}_4$ -based composites were highly enhanced to compare with those of pristine  $\text{g-C}_3\text{N}_4$ . The valence band and conduction band of  $\text{g-C}_3\text{N}_4$  are about  $-0.90$  and  $+1.80$  eV [15,23]. And thus, it is likely to form new heterostructure between cotton-like  $\text{g-C}_3\text{N}_4$  and the self-doped  $\text{Ta}_2\text{O}_5$  to promote the charge separation because of the well matched band structures [27].

In this work, we successfully prepared a novel  $\text{Ta}^{4+}$  self-doped  $\text{Ta}_2\text{O}_5$  quantum dots and TCN catalysts by vapor hydrolysis reaction and calcining treatment for the first time. The photocatalytic activities for hydrogen production and RhB photodegradation of TCN catalyst were highly enhanced mainly because of the formation of  $\text{Ta}-\text{O}-\text{C}$  chemical bond, which highly enhanced the charge separation between the self-doped  $\text{Ta}_2\text{O}_5$  and cotton-like  $\text{g-C}_3\text{N}_4$ . The possible direct Z-scheme mechanisms of TCN catalyst for hydrogen production and RhB degradation were also investigated in detail.

## 2. Experimental

### 2.1. Sample preparation

All the chemicals were commercially available and directly used without any treatment. The self-doped  $\text{Ta}_2\text{O}_5$  quantum dots were prepared by vapor hydrolysis reaction in this experiment. In a typical procedure, 8 mL distilled water was added into a Teflon line, and 0.50 g  $\text{Ta}(\text{C}_2\text{H}_5\text{O})_5$  was dissolved in 6 mL ethylene glycol in an inner container and transferred into the Teflon line. Then the autoclave was sealed and heated at 220 °C for 20 h. The product was separated from some impurity and ethylene glycol by centrifugation, washed

with ethanol and distilled water several times, and then dried at  $\sim 60$  °C for 48 h.

The  $\text{g-C}_3\text{N}_4$  was fabricated by calcining treatment according to the literature with slight modifications [15]. Typically, melamine was put into a covered ceramic crucible and heated to 550 °C at a rate of 0.5 °C/min in a muffle furnace for 4 h, naturally cooled, and then the  $\text{g-C}_3\text{N}_4$  was obtained.

TCN catalysts were successfully prepared by a facile calcining method. At first, the as-prepared  $\text{g-C}_3\text{N}_4$  with different amount of the self-doped  $\text{Ta}_2\text{O}_5$  quantum dots were mixed and grinded, then the mixtures were transferred into a ceramic crucible with a cover and heated at 500 °C at a heating rate of 2 °C/min for 3 h, naturally cooled, then TCN catalyst was obtained. The samples with the different mass ratio ( $\text{g-C}_3\text{N}_4/\text{Ta}_2\text{O}_5$ ) of 1:1, 4:1, 6:1 and 8:1 were denoted as TCN-1, TCN-4, TCN-6, and TCN-8, respectively. For comparison, the mixed sample with mass ratio ( $\text{g-C}_3\text{N}_4/\text{Ta}_2\text{O}_5$ ) of 6:1 without calcining treatment was denoted as TCN-mix. And Scheme 1 showed the formation procedure of self-doped  $\text{Ta}_2\text{O}_5$  quantum dots and TCN catalyst.

### 2.2. Characterization

The morphologies of  $\text{g-C}_3\text{N}_4$  and TCN-6 photocatalyst were investigated by cold field emission Scanning electron microscope (SEM) (Hitachi, SU8010) and Transmission electron microscope (TEM) (Tecnai, G2F30) and HRTEM at 300 kV. The crystal structure was investigated by X-ray diffraction (XRD) (PANalytical, X'Pert PRO) with  $\text{Cu K}\alpha$  radiation ( $\lambda = 0.15406$  nm). The chemical structure and the element chemical states of the as-prepared  $\text{Ta}_2\text{O}_5$  and TCN catalyst were studied on a Fourier-transform infrared spectroscopy (FT-IR) (Thermo Nicolet Corporation, Avatar 360) and X-ray photoelectron spectroscopy (XPS) (Thermo Fisher Scientific, ESCALAB 250Xi). The UV-vis absorption spectra of commercial  $\text{Ta}_2\text{O}_5$ , the self-doped  $\text{Ta}_2\text{O}_5$ ,  $\text{g-C}_3\text{N}_4$  and TCN catalysts were determined by double-beam ultraviolet-visible spectrophotometer (Beijing's general instrument co., LTD, TU-1900) with  $\text{BaSO}_4$  as reference standard. Photoluminescence emission spectra (PL) was carried out on a FluoroMax-4 photoluminescence instrument (HORIBA Jobin Yvon) with  $\text{g-C}_3\text{N}_4$ , and the self-doped  $\text{Ta}_2\text{O}_5$  quantum dots and TCN catalysts were dissolved in ethyl alcohol and treated by ultrasound for 30 min. The uncoupled electron properties of commercial  $\text{Ta}_2\text{O}_5$ ,  $\text{g-C}_3\text{N}_4$ , the self-doped  $\text{Ta}_2\text{O}_5$  and TCN catalysts were investigated on an Electron paramagnetic resonance spectrometer (EPR) (at 90 K (Bruker Corporation, A300-10/12).

### 2.3. Photocatalytic hydrogen production

Photocatalytic hydrogen production tests were conducted under 300 W Xe lamp using a 420 nm cut-off filter. The reaction was conducted in a sealed gas circulation and evacuation system (LabSolar-III AG, Beijing PerfectLight Co., Ltd., China). The reactor was placed under the Xe lamp for photocatalytic experiment. In a typical procedure, 0.05 g TCN catalyst with 3 wt.% Pt co-catalyst was added into a mixture of 10 mL triethanolamine (TEOA) and 90 mL distilled water. After sealing the reactor and the pressure achieving a balance, the reactor was then irradiated for 60 min to photodeposit  $\text{H}_2\text{PtCl}_6\cdot(\text{H}_2\text{O})_6$  onto TCN catalyst by a 300 W Xe lamp (PLS SXE300C, Beijing PerfectLight Co., Ltd., China). Then pumping the  $\text{H}_2$  produced in the photodeposition process and the pressure achieving a balance again, the reactor was irradiated by 300 W Xe lamp (MicroSolar300) using a 420 nm cut-off filter for 120 min. The amount of hydrogen production was measured by gas chromatograph (Techcomp, 7890 II) with a TCD detector (molecular sieve 5 Å column) and Ar as carrier gas. The hydrogen production activity of the self-doped  $\text{Ta}_2\text{O}_5$  was measured under 300 W Xe lamp using a 400 nm cut-off filter with 3 wt.% Pt co-catalyst.

### 2.4. Photodegradation experiment

The photocatalytic activities of TCN catalysts for RhB degradation were evaluated under visible light irradiation using a 300 W Xe lamp (MicroSolar 300, Beijing PerfectLight Co., Ltd., China) with a 420 nm cut-off filter. In a typical procedure, 0.10 g TCN catalyst was mixed with RhB solution (10 mg/L) and stirred for 30 min in the dark to achieve an adsorption–desorption equilibrium. Then the reaction system was irradiated using a 300 W Xe lamp (MicroSolar300) with a 420 nm cut-off filter and the reaction solution was collected every 10 min for analyzing by UV–vis spectrophotometer (Shanghai Spectrum Instruments Co., Ltd, 722E). The recyclable photocatalytic activity test was also carried out, and the photocatalyst was collected by centrifuging after each run, and used for next run. Besides, the trapping experiments of TCN-6 catalyst with addition of 0.1 g ammonium oxalate or 2 mL isopropanol for RhB degradation were also carried out to investigate the main active species under visible light irradiation ( $\lambda > 420$  nm).

### 2.5. Photoelectrochemical tests

The photocurrent transient response and electrochemical impedance spectra of  $\text{g-C}_3\text{N}_4$ , the self-doped  $\text{Ta}_2\text{O}_5$  and TCN-6 catalysts were determined on a CHI660D electrochemical working station (shanghai, Chen hua) with a three-compartment cell. A 300 W Xe lamp (PLS SXE300C) with a 420 nm cutoff filter was employed as the visible light resource. The electrodes of the catalysts, Ag/AgCl electrode and Pt wire electrode were as the working electrode, counter electrode and reference electrode, respectively, and 0.1 M  $\text{Na}_2\text{SO}_4$  solution was served as electrolyte. The electrode was prepared by an electrophoretic deposition method with slight modifications [29]. 25 mg catalyst was dispersed in 50 mL isopropyl alcohol with a small amount of  $\text{Mg}(\text{NO}_3)_2$  (0.0074 g) and treated with ultrasound for 30 min. The ITO glass was used as working electrode with a Pt sheet as counter electrode. The electrophoretic deposition was carried out for 3 min with a 50 V direct-current voltage, and then the prepared electrode was naturally dried at room temperature for use.

## 3. Result and discussion

The morphologies and nanostructure of pure  $\text{g-C}_3\text{N}_4$  and TCN-6 catalyst were investigated via SEM, TEM and HRTEM. As depicted in Fig. 1(a), pure  $\text{g-C}_3\text{N}_4$  was a typical block-shaped morphology

with layered structures. The size of  $\text{g-C}_3\text{N}_4$  grain was approximately 2–3  $\mu\text{m}$ . Fig. 1(b) also clearly revealed the surface morphology of  $\text{g-C}_3\text{N}_4$ . The insert in Fig. 1(b) confirmed the formation of  $\text{g-C}_3\text{N}_4$ . Fig. 1(c) showed the microscopic morphology of TCN-6 catalyst with a relatively homogeneous distribution of  $\text{Ta}_2\text{O}_5$  nanoparticle incorporated in the cotton-like  $\text{g-C}_3\text{N}_4$ , appearing as the soft cotton-like  $\text{g-C}_3\text{N}_4$  modified by the self-doped  $\text{Ta}_2\text{O}_5$ . The laminar cotton-like  $\text{g-C}_3\text{N}_4$  contributed to the increase of the specific surface area [30]. As depicted in Fig. 1(d), the HRTEM image of the TCN-6 catalyst showed an interplanar spacing of 0.386 nm with the particle size of the self-doped  $\text{Ta}_2\text{O}_5$  less than 10 nm, which was ascribed to the (001) crystal interplanar of  $\text{Ta}_2\text{O}_5$  and further confirmed the formation of the self-doped  $\text{Ta}_2\text{O}_5$  quantum dots. Besides, the high magnification TEM images of TCN-6 catalyst in Fig. S1 (b) also confirmed the existence of  $\text{Ta}_2\text{O}_5$  quantum dots in the TCN catalyst. The inset of electron diffraction of Fig. 1(d) clearly revealed the poor crystallization of TCN-6 catalyst. Fig. 1(e, f) showed the high-angle annular dark field and the scanning transmission electron (HAADF-STEM) image and the corresponding elemental mapping of TCN-6 catalyst. Fig. 1(e) further revealed the cotton-like morphology of TCN catalyst, which was consistent with the SEM image of TCN-6 catalyst in Fig. S1 (a). Fig. 1(f) clearly revealed that TCN-6 catalyst was composed of carbon, nitrogen, oxygen and tantalum elements, which were uniformly distributed over the entire TCN-6 catalyst, indicating the relatively homogeneous distribution of the self-doped  $\text{Ta}_2\text{O}_5$  over the cotton-like  $\text{g-C}_3\text{N}_4$ .

Fig. 2 showed the XRD patterns of  $\text{g-C}_3\text{N}_4$ , the self-doped  $\text{Ta}_2\text{O}_5$ , TCN-1, TCN-4, TCN-6 and TCN-8 catalysts. The XRD pattern of  $\text{g-C}_3\text{N}_4$  showed two distinct diffraction peaks at around 13.0° and 27.4°, which were indexed for the (100) and (002) planes of  $\text{g-C}_3\text{N}_4$  [23,31], corresponding to the in-plane structural packing motif of tris-triazine units and inter-planar stacking peak of aromatic system [32]. The XRD pattern of the self-doped  $\text{Ta}_2\text{O}_5$  showed one distinct and broad diffraction peaks at around 22.9°, corresponding to the (001) plane of  $\text{Ta}_2\text{O}_5$  (JCPDS No.25-0922), which was in good agreement with HRTEM results and further confirmed the formation of  $\text{Ta}_2\text{O}_5$ . The other diffraction peaks were slightly weaker for  $\text{Ta}_2\text{O}_5$  because of its relatively poor crystallinity under the low reaction temperature, but the characteristic diffraction peaks of  $\text{Ta}_2\text{O}_5$  existed, and well agreed with the standard card of JCPDS No.25-0922. The average crystallite size of the self-doped  $\text{Ta}_2\text{O}_5$  was 8.92 nm according to Debye–scherer's equation, further confirming the formation of the self-doped  $\text{Ta}_2\text{O}_5$  quantum dots, which was also consistent with the HRTEM results. The diffraction peaks of  $\text{g-C}_3\text{N}_4$  and  $\text{Ta}_2\text{O}_5$  were also observed in TCN-1, TCN-4, TCN-6 and TCN-8 catalysts. The relative diffraction intensity of (100) and (002) planes of  $\text{g-C}_3\text{N}_4$  became stronger with the mass ratio increase of  $\text{g-C}_3\text{N}_4$ , while the relative diffraction peak intensity of (001) plane of  $\text{Ta}_2\text{O}_5$  increased with the decreasing of the mass ratio of  $\text{g-C}_3\text{N}_4$  regularly. The regular changes of the diffraction intensity had been reported for  $\text{BiVO}_4/\text{g-C}_3\text{N}_4$  [33] and  $\text{CeO}_2/\text{g-C}_3\text{N}_4$  [27]. And we might conclude the coupling of (100) and (002) planes of  $\text{g-C}_3\text{N}_4$  and (001) planes of the self-doped  $\text{Ta}_2\text{O}_5$  established a closely interface [27,34], which was also consistent with the HRTEM analyses. And thus, the above analyses further confirmed the formation of TCN catalyst.

Fig. 3 showed the FT-IR spectra of the self-doped  $\text{Ta}_2\text{O}_5$ ,  $\text{g-C}_3\text{N}_4$ , TCN-1, TCN-4, TCN-6 and TCN-8 catalysts. The absorption peak of the self-doped  $\text{Ta}_2\text{O}_5$  at 3460  $\text{cm}^{-1}$  could be attributed to the –OH of carbon materials or the absorbed water molecules [35,36]. The broad absorption peak of  $\text{g-C}_3\text{N}_4$  at 3150  $\text{cm}^{-1}$  was ascribed to the stretching vibration of N–H and O–H derived from melamine polymerization and absorbed water molecule, respectively [36,37]. The absorption peaks at 2931 and 2877  $\text{cm}^{-1}$  was assigned to the skeletal vibration of  $\text{sp}^2$  and  $\text{sp}^3$  C–H [38,39]. The

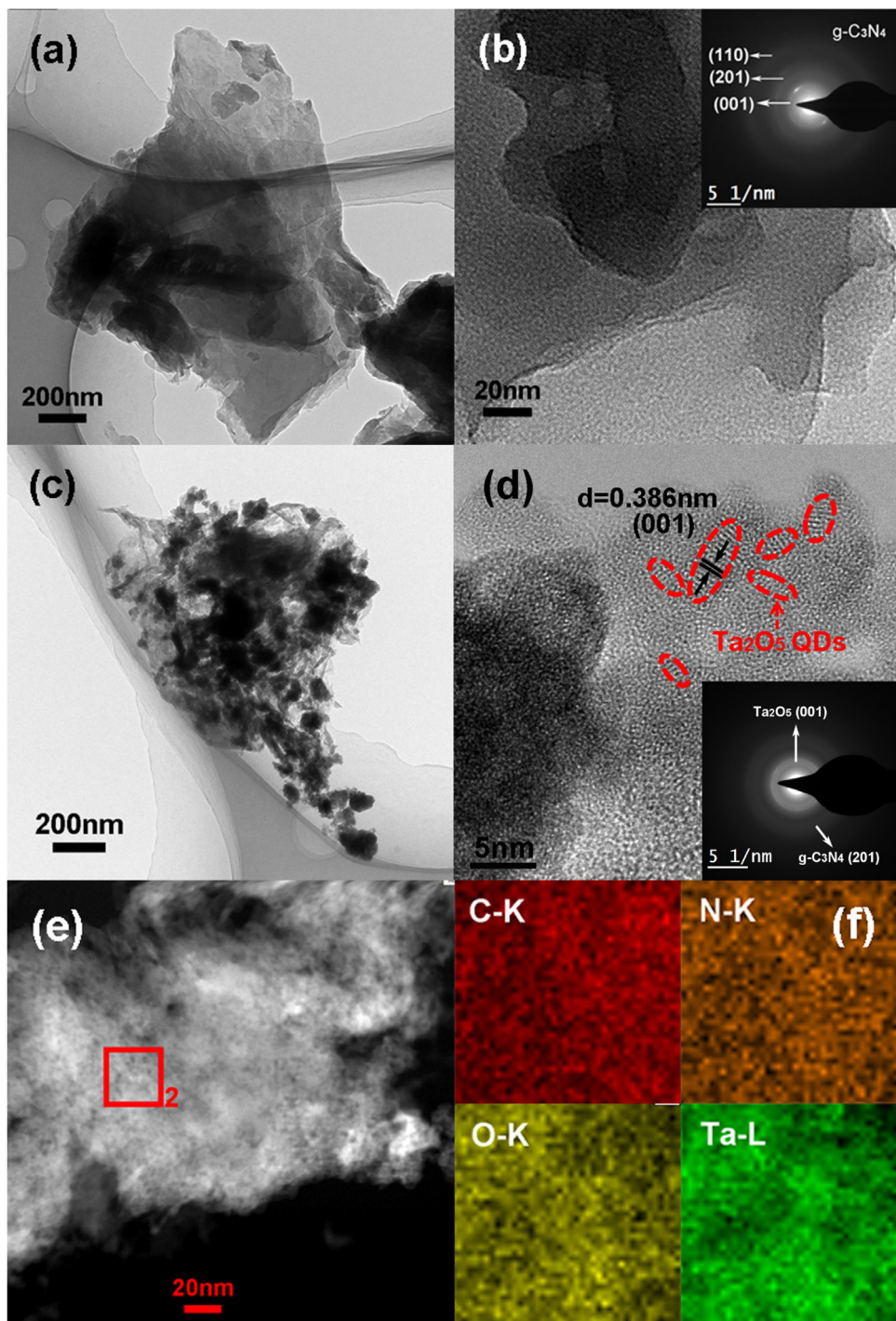


**Fig. 1.** Typical TEM, HRTEM images of  $\text{g-C}_3\text{N}_4$  (a, b) and TCN (c, d) catalysts; HAADF-STEM image (e) and the corresponding EDS mapping (f) of TCN catalyst.

peak located at  $1593\text{ cm}^{-1}$  was attributed to the hydrogen-bonded carbonyl stretching, indicating the formation of carbon-related compounds in the vapor hydrolysis reaction. The absorption peaks at  $850\text{--}1800\text{ cm}^{-1}$  was attributed to the typical stretching vibration of CN heterocycles [27]. The peak at  $808\text{ cm}^{-1}$  was attributed to the breathing mode of triazine units [31], which further confirmed the formation of  $\text{g-C}_3\text{N}_4$ . The broad absorption peak at  $645\text{ cm}^{-1}$  was attributed to the combination of Ta—O and Ta—O-Ta bonds vibrations [35,40,41]. For TCN catalyst, the broad absorption band at  $645\text{ cm}^{-1}$  of Ta—O-Ta and Ta—O confirmed the existence of  $\text{Ta}_2\text{O}_5$  in the as-prepared TCN catalysts [35,40–42]. And the broad absorption

band for TCN-1, TCN-4, TCN-6 and TCN-8 catalysts at  $645\text{ cm}^{-1}$  had a slight red shift with the mass ratio increasing of the self-doped  $\text{Ta}_2\text{O}_5$  [33,37]. It was obviously that the absorption peak intensity of triazine units at  $808\text{ cm}^{-1}$  of TCN-1, TCN-4, TCN-6 and TCN-8 catalysts increased regularly with the mass ratio increase of  $\text{g-C}_3\text{N}_4$ . And thus, it could be concluded that TCN catalyst was successfully fabricated using  $\text{Ta}(\text{C}_2\text{H}_5\text{O})_5$  and melamine as the precursors.

Fig. 4 showed the high-resolution XPS spectra of C1s, N1s, O1s and Ta 4f to further investigate the elemental chemical states and composition of  $\text{g-C}_3\text{N}_4$ , the self-doped  $\text{Ta}_2\text{O}_5$  and TCN catalyst. As shown in Fig. 4(a), the C1s peak for  $\text{Ta}_2\text{O}_5$  at 284.7 eV was ascribed

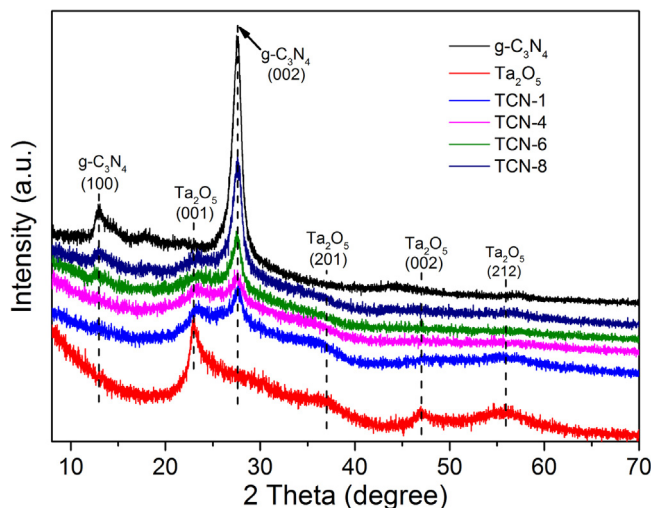


Fig. 2. XRD patterns of  $\text{g-C}_3\text{N}_4$ , the self-doped  $\text{Ta}_2\text{O}_5$ , and TCN catalysts.

to adventitious carbon [43], and the peak at 286.0 eV was attributed to the carbon-compounds, seeming like carbon in the graphite intercalation compounds produced from ethylene glycol [35,44], which might be in favour of visible light absorption for the self-doped  $\text{Ta}_2\text{O}_5$ , and the similar phenomenon was reported in carbon modified  $\text{NaTaO}_3$  mesocrystal [35]. The C1s peaks at 284.9 eV for pure  $\text{g-C}_3\text{N}_4$  and TCN-6 catalysts were ascribed to surface adventitious carbon, and the peaks at 288.6 and 288.4 eV for pure  $\text{g-C}_3\text{N}_4$  and TCN-6 were ascribed to the  $\text{sp}^2\text{C}$  bonded in  $\text{N}-\text{C}=\text{N}$  of  $\text{g-C}_3\text{N}_4$  [45]. In Fig. 4(b), the N1s peaks for  $\text{g-C}_3\text{N}_4$  at 398.9, 399.9 and 401.5 eV could be assigned to the pyridinic-like nitrogen ( $\text{N}-\text{sp}^2\text{C}$ ), graphitic nitrogen ( $\text{N}-(\text{C})_3$ ) and amino groups ( $\text{C}-\text{N}-\text{H}$ ), respectively [27,37]. The N1s of TCN-6 catalyst displayed slightly lower binding energies (398.8, 399.8 and 401.3 eV) compared with those of  $\text{g-C}_3\text{N}_4$  because of the strong interaction between  $\text{Ta}_2\text{O}_5$  and  $\text{g-C}_3\text{N}_4$  [46]. In Fig. 4(c), O1s for the self-doped  $\text{Ta}_2\text{O}_5$  could be fitted

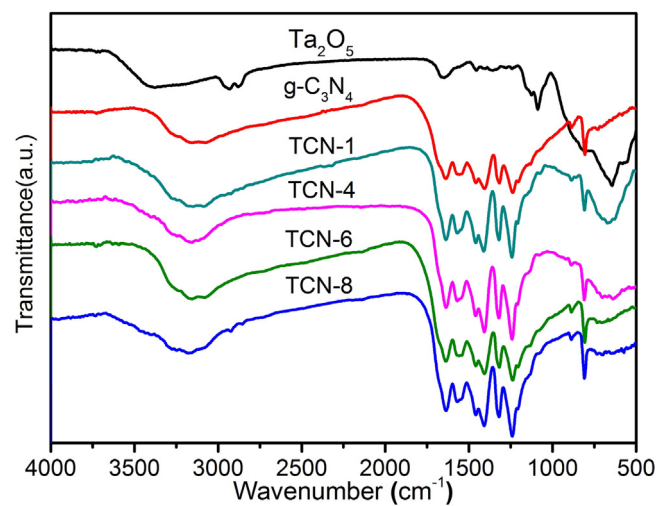


Fig. 3. FT-IR spectra of the self-doped  $\text{Ta}_2\text{O}_5$ ,  $\text{g-C}_3\text{N}_4$ , TCN-1, TCN-4, TCN-6 and TCN-8 catalysts.

into two peaks at 530.7 and 532.3 eV, which were attributed to the lattice oxygen atoms, oxygen atoms of surface  $-\text{OH}$  species and oxygen vacancy neighbors to  $\text{Ta}^{4+}$  species of the self-doped  $\text{Ta}_2\text{O}_5$  catalyst [37,47,48]. The binding energies of O1s (530.7, 532.3 eV) of TCN-6 catalyst were slightly higher compared with that of  $\text{Ta}_2\text{O}_5$ . Interestingly, the binding energies of  $\text{Ta}4\text{f}_{7/2}$  and  $\text{Ta}4\text{f}_{5/2}$  for TCN-6 catalyst (26.5, 28.4 eV) (Fig. 4(d)) were also higher compared with those of the self-doped  $\text{Ta}_2\text{O}_5$  and TCN-mix, further confirming the formation of new chemical bond  $\text{Ta}-\text{O}-\text{C}$  in TCN-6 catalyst [27,37,38,49]. In literatures,  $\text{Ti}-\text{O}-\text{C}$  chemical bond was often thought to be formed because of the peaks of  $\text{Ti}(2\text{p}_{1/2})$  and  $\text{Ti}(2\text{p}_{3/2})$  shifting towards a higher binding energy [38,50], while the chemical bonds in the  $\text{g-C}_3\text{N}_4/\text{NaNbO}_3$  catalyst was also thought to be formed because the binding energies of  $\text{Nb}3\text{d}_{3/2}$ ,  $\text{Nb}3\text{d}_{5/2}$ , and O1s of  $\text{g-C}_3\text{N}_4/\text{NaNbO}_3$  decreased compared with that of the pure  $\text{NaNbO}_3$  [51]. Besides, the  $\text{Ta}4\text{f}_{7/2}$  peak of the as-prepared  $\text{Ta}_2\text{O}_5$

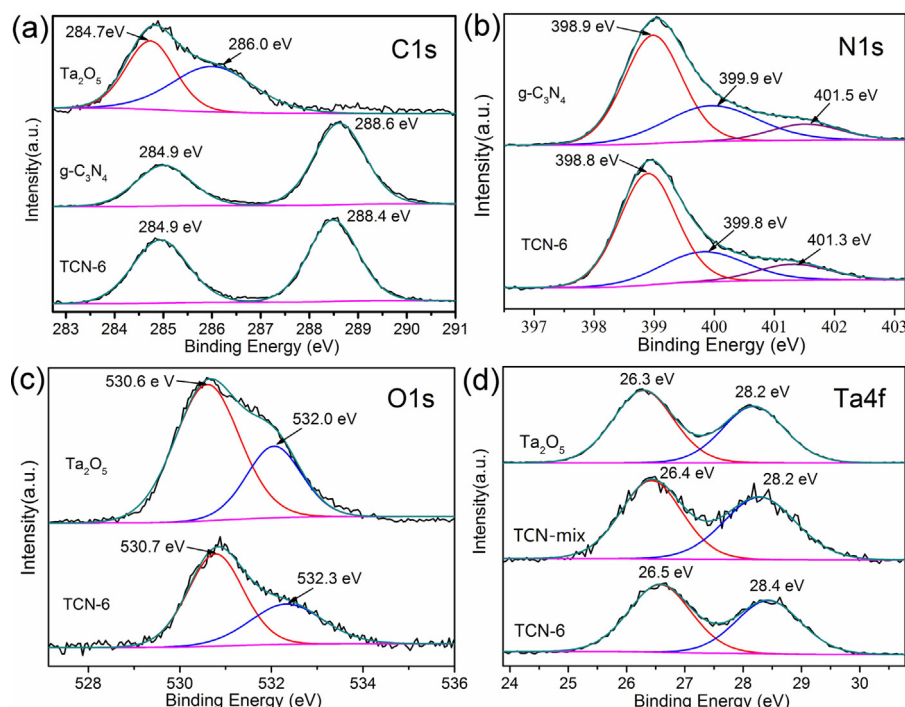
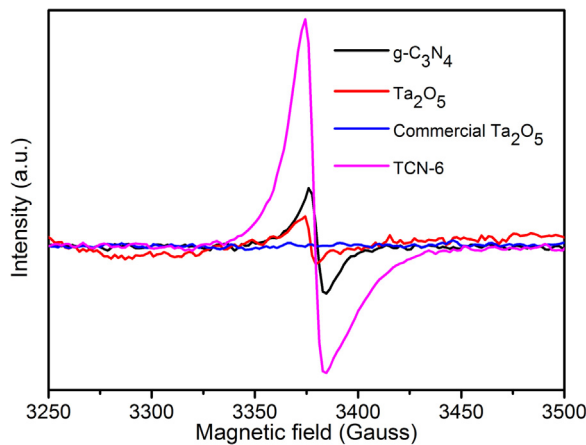


Fig. 4. XPS spectra of the self-doped  $\text{Ta}_2\text{O}_5$ ,  $\text{g-C}_3\text{N}_4$ , TCN-mix and TCN catalysts: (a) C1s, (b) N1s, (c) O1s and (d) Ta 4f.



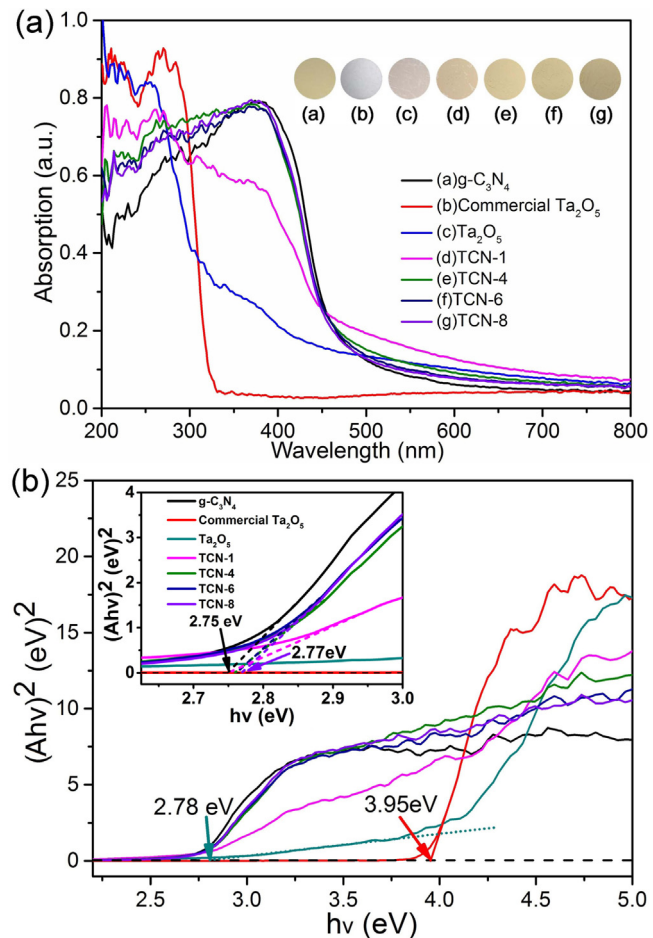
**Fig. 5.** EPR spectra of  $\text{g-C}_3\text{N}_4$ , the self-doped  $\text{Ta}_2\text{O}_5$ , commercial  $\text{Ta}_2\text{O}_5$ , and TCN catalysts.

(26.3 eV) was lower than that of the non-defect  $\text{Ta}_2\text{O}_5$  reported in literature [52], indicating the formation of  $\text{Ta}^{4+}$  species neighbors to oxygen vacancy in the self-doped  $\text{Ta}_2\text{O}_5$  [47,53], as discussed below. Based on the above analyses, it could be concluded that TCN catalyst was successfully fabricated by forming  $\text{Ta}-\text{O}-\text{C}$  bond rather than the simple physical mixture.

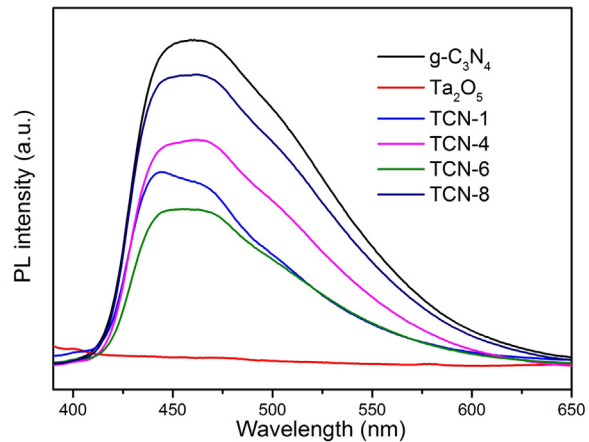
EPR measurements were conducted to further investigate the oxygen vacancy defects (or  $\text{Ta}^{4+}$  species) of  $\text{g-C}_3\text{N}_4$ , commercial  $\text{Ta}_2\text{O}_5$ , the self-doped  $\text{Ta}_2\text{O}_5$ , and TCN catalysts. As shown in Fig. 5, the commercial  $\text{Ta}_2\text{O}_5$  showed no detectable EPR signals, whereas the as-prepared  $\text{Ta}_2\text{O}_5$  quantum dots displayed a strong EPR signal at about  $g = 2.085$ , which could be attributed to oxygen vacancy (Ov.) defects ( $\text{Ta}^{4+}$  species) in the as-prepared  $\text{Ta}_2\text{O}_5$ , because  $\text{Ta}^{4+}$  species was often thought to be produced as well as oxygen vacancy (Ov.) generation [47,54]. The  $\text{g-C}_3\text{N}_4$  showed an EPR signal at about  $g = 2.083$ , which was corresponding to the uncoupled electron of the skeleton CN aromatic rings [24]. The highly enhanced EPR signal in intensity of TCN catalyst was observed at  $g = 2.084$ , which indicated that the  $\text{Ta}-\text{O}-\text{C}$  chemical bond contributed to the existence of  $\text{Ta}^{4+}$  species in the TCN catalyst.

Fig. 6 displayed the UV-vis absorbance spectrum, the colors (insert) and the estimated bandgap of the commercial  $\text{Ta}_2\text{O}_5$ , the self-doped  $\text{Ta}_2\text{O}_5$ ,  $\text{g-C}_3\text{N}_4$ , TCN-1, TCN-4, TCN-6 and TCN-8 catalysts. As displayed in Fig. 6(a), the commercial  $\text{Ta}_2\text{O}_5$  exhibited strong UV absorption with a spectrum absorption edge of  $\sim 320$  nm, and the estimated bandgap of the commercial  $\text{Ta}_2\text{O}_5$  is about 3.95 eV, which was consistent with the literature [11]. However, the self-doped  $\text{Ta}_2\text{O}_5$  showed a strong visible light absorption, which was induced by  $\text{Ta}^{4+}$  species in self-doped  $\text{Ta}_2\text{O}_5$  [35], showing great advantages compared with those of commercial  $\text{Ta}_2\text{O}_5$ , and the estimated bandgap of the as-prepared  $\text{Ta}_2\text{O}_5$  in this experiment was  $\sim 2.78$  eV, much lower than that of commercial  $\text{Ta}_2\text{O}_5$  (Fig. 6(b)), which indicated that the self-doped  $\text{Ta}_2\text{O}_5$  were likely to have visible light activities. Besides, TCN-1, TCN-4, TCN-6 and TCN-8 catalysts also displayed strong visible light absorption from 400 to 800 nm, mainly because of the existence of  $\text{g-C}_3\text{N}_4$  [55]. And the estimated bandgaps of TCN-1, TCN-4, TCN-6 and TCN-8 catalysts were about 2.753, 2.759, 2.765, 2.770 eV, which were higher than that of  $\text{g-C}_3\text{N}_4$  ( $\sim 2.75$  eV) yet much lower than that of the commercial  $\text{Ta}_2\text{O}_5$  (3.95 eV). Besides, the spectral absorption edge of TCN-1, TCN-4, TCN-6 and TCN-8 had a distinct blue shift in comparison to that of  $\text{g-C}_3\text{N}_4$ , mainly because of the formation of  $\text{Ta}-\text{O}-\text{C}$  chemical bond between the self-doped  $\text{Ta}_2\text{O}_5$  and cotton-like  $\text{g-C}_3\text{N}_4$ .

The PL emission spectra of  $\text{g-C}_3\text{N}_4$ , the self-doped  $\text{Ta}_2\text{O}_5$ , TCN-1, TCN-4, TCN-6 and TCN-8 catalysts excited by 350 nm ultraviolet light were measured to study the trapping, migration, and



**Fig. 6.** UV-vis absorption spectra, the colors (insert) and estimated bandgaps of the self-doped  $\text{Ta}_2\text{O}_5$ ,  $\text{g-C}_3\text{N}_4$ , TCN-1, TCN-4, TCN-6 and TCN-8 catalysts.



**Fig. 7.** Photoluminescent spectra of  $\text{g-C}_3\text{N}_4$ , the self-doped  $\text{Ta}_2\text{O}_5$ , TCN-1, TCN-4, TCN-6 and TCN-8 catalysts.

recombination of the photo-induced electrons and holes at room temperature [37,56]. As shown in Fig. 7, the PL emission spectra of  $\text{g-C}_3\text{N}_4$  presented a strong band-band emission from  $\sim 390$  to 650 nm, indicating the rapid recombination of the photo-induced electrons and holes, which was detrimental for enhancement of the charge separation efficiency. However, the PL intensity of TCN catalysts significantly decreased, and TCN-6 displayed the lowest PL intensity, indicating that the recombination of the photo-induced electrons and holes was highly suppressed because of the formation

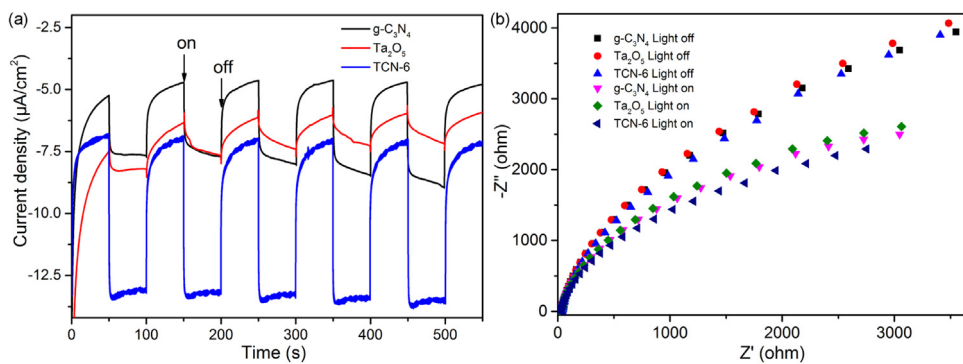
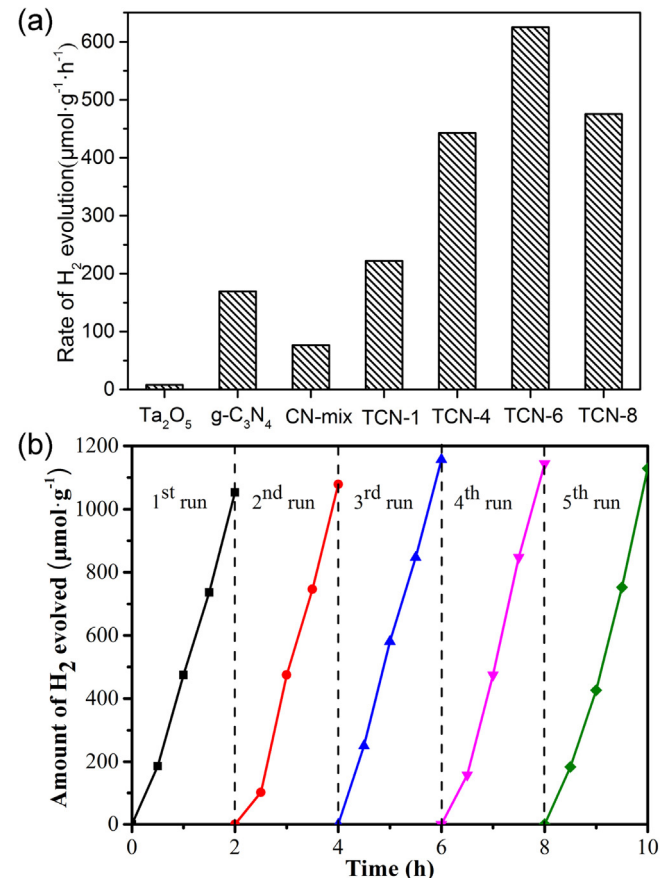


**Fig. 8.** Photocurrent response (a) and electrochemical impedance spectra (b) of g-C<sub>3</sub>N<sub>4</sub>, the self-doped Ta<sub>2</sub>O<sub>5</sub>, TCN-6 catalysts under visible light irradiation ( $\lambda > 420$  nm) at 0.1 V vs. Ag/AgCl in 0.1 M Na<sub>2</sub>SO<sub>4</sub> solution.

of Ta—O—C bond and Ta<sup>4+</sup> species, which benefited of the excited electrons easily transferring into the interface between cotton-like g-C<sub>3</sub>N<sub>4</sub> and Ta<sub>2</sub>O<sub>5</sub> [14,57,58]. And thus, it was the formation of Ta—O—C chemical bond and Ta<sup>4+</sup> species between the self-doped Ta<sub>2</sub>O<sub>5</sub> and cotton-like g-C<sub>3</sub>N<sub>4</sub> that highly promoted the charge separation.

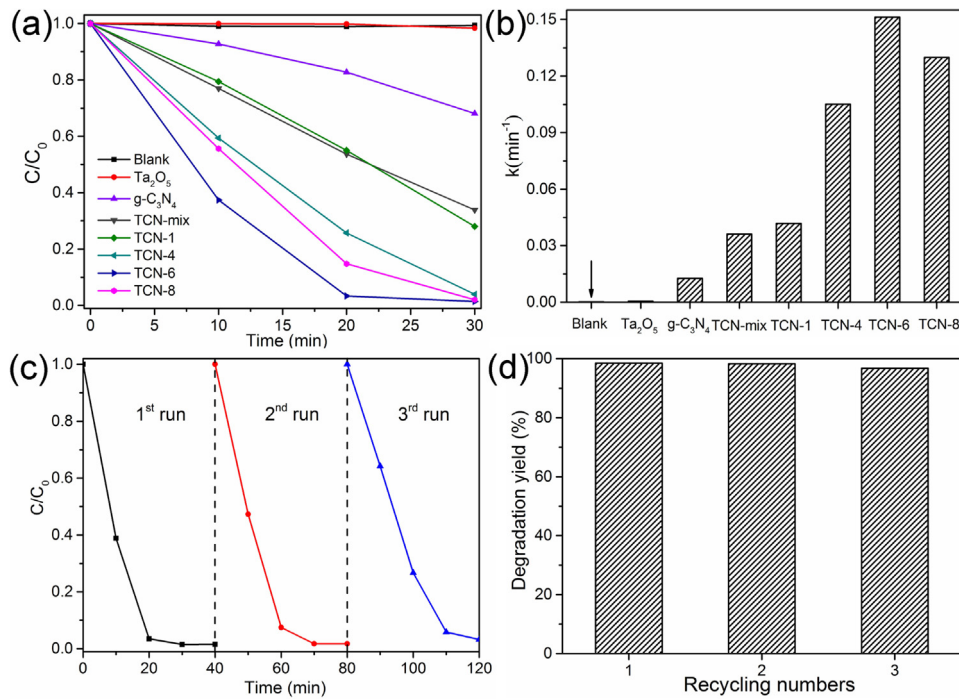
In order to further investigate the interfacial charge separation and charge transfer resistance of g-C<sub>3</sub>N<sub>4</sub>, the self-doped Ta<sub>2</sub>O<sub>5</sub> and TCN catalyst, photocurrent transient response and electrochemical impedance spectra were determined under visible light irradiation ( $\lambda > 420$  nm) with a three-compartment cell. In general, the enhanced photocurrent response and small arc radius often represented a higher separation efficiency of photo-induced electron and photo-induced hole pairs and lower charge transfer resistance [59]. As shown in Fig. 8(a), the generated photocurrent of g-C<sub>3</sub>N<sub>4</sub>, the self-doped Ta<sub>2</sub>O<sub>5</sub> and TCN-6 catalysts displayed a reproducible response during the light source on/off cycles. And TCN-6 catalyst displayed the strongest photocurrent transient response to compare with those of g-C<sub>3</sub>N<sub>4</sub> and the self-doped Ta<sub>2</sub>O<sub>5</sub>, which indicated the photo-induced electrons and holes could effectively separate and transfer under visible light irradiation ( $\lambda > 420$  nm) [60]. As depicted in Fig. 8(b), the arc radii of g-C<sub>3</sub>N<sub>4</sub>, the self-doped Ta<sub>2</sub>O<sub>5</sub> and TCN-6 catalysts under visible light irradiation was much smaller than those of g-C<sub>3</sub>N<sub>4</sub>, the self-doped Ta<sub>2</sub>O<sub>5</sub> and TCN-6 catalysts without irradiation, indicating smaller charge transfer resistance, lower recombination of photo-induced electrons and photo-induced holes and higher charge separation efficiency under visible light irradiation [57,61]. Besides, TCN-6 catalyst displayed the smallest arc radius, indicating the smallest charge transfer resistance and highest charge separation efficiency under visible light irradiation, which further confirmed that the formation of Ta—O—C chemical bond in TCN catalyst highly enhanced the charge separation between the self-doped Ta<sub>2</sub>O<sub>5</sub> and cotton-like g-C<sub>3</sub>N<sub>4</sub>.

Fig. 9 showed the photocatalytic hydrogen evolution activities of the self-doped Ta<sub>2</sub>O<sub>5</sub>, g-C<sub>3</sub>N<sub>4</sub>, TCN-mix, TCN-1, TCN-4, TCN-6 and TCN-8 catalysts and further confirmed the enhancement of the photocatalytic activity of TCN catalyst to compare with those of the self-doped Ta<sub>2</sub>O<sub>5</sub>, g-C<sub>3</sub>N<sub>4</sub> and the g-C<sub>3</sub>N<sub>4</sub>-based photocatalysts in table S1 (Supporting information). As depicted in Fig. 9(a), the hydrogen production rate of the self-doped Ta<sub>2</sub>O<sub>5</sub> could reach 7.98 μmol g<sup>-1</sup> h<sup>-1</sup> because of the formation of Ta<sup>4+</sup> defect energy level in the Ta<sub>2</sub>O<sub>5</sub>, while the commercial Ta<sub>2</sub>O<sub>5</sub> displayed no visible light photocatalytic activity. The pure g-C<sub>3</sub>N<sub>4</sub> showed a hydrogen evolution rate of 169.45 μmol g<sup>-1</sup> h<sup>-1</sup>, much lower than those of all the TCN catalysts. And TCN-6 catalyst displayed the highest photocatalytic hydrogen evolution activity (624.99 μmol g<sup>-1</sup> h<sup>-1</sup>), also higher than that of g-C<sub>3</sub>N<sub>4</sub> calcined by the second time at 500 °C for 3 h (~282.07 μmol g<sup>-1</sup> h<sup>-1</sup>), which also indicated that the highly enhanced photocatalytic activities of TCN catalysts were mainly



**Fig. 9.** The photocatalytic hydrogen evolution rate of the self-doped Ta<sub>2</sub>O<sub>5</sub>, g-C<sub>3</sub>N<sub>4</sub>, TCN-mix, TCN-1, TCN-4, TCN-6 and TCN-8 catalysts, and recyclable photocatalytic activity of TCN-6 catalyst.

attributed to the doping effects of the self-doped Ta<sub>2</sub>O<sub>5</sub> quantum dots, though the secondary calcination of g-C<sub>3</sub>N<sub>4</sub> in a ceramic crucible with a cover was also favorable for the increase of the photocatalytic activity [62]. And thus, we could conclude that Ta<sub>2</sub>O<sub>5</sub> quantum dots played a crucial role for enhancing the photocatalytic activities of TCN catalysts. Besides, all the photocatalytic hydrogen evolution activities of TCN catalysts were much higher than that of TCN-mix (6:1 sample), mainly because of the formation of Ta—O—C chemical bond between the self-doped Ta<sub>2</sub>O<sub>5</sub> and g-C<sub>3</sub>N<sub>4</sub> rather than the only simple physical mixture. We also investigated the photocatalytic stability of TCN-6 catalyst for photocatalytic hydrogen evolution under visible light irradiation. As shown in Fig. 9 (b),

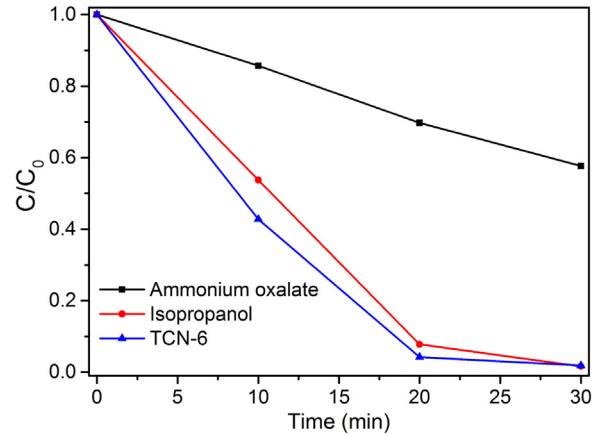


**Fig. 10.** Photocatalytic activities (a), the rate constant (b), three recyclable runs (c) of TCN-6 catalyst and the degradation yield (d) of TCN-6 catalyst for RhB degradation.

TCN-6 catalyst still displayed excellent photocatalytic activity even after five recyclable tests.

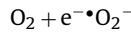
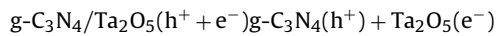
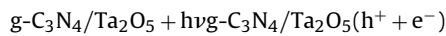
We also carried out the photocatalytic RhB degradation of TCN catalysts under visible light irradiation to evaluate the charge separation between the self-doped  $Ta_2O_5$  and cotton-like  $g-C_3N_4$ . Fig. 10(a) showed the photocatalytic RhB degradation curves for 30 min. The pure  $g-C_3N_4$  displayed relatively poor visible light degradation activity compared with those of all the TCN catalysts. Besides, almost all the RhB could be removed in about 20 min for TCN-6 catalyst, much faster than those of TCN-mix,  $g-C_3N_4$ , the self-doped  $Ta_2O_5$ , and the  $g-C_3N_4$ -based catalysts in table S2 (Supporting information), further confirming the formation of the Ta—O—C chemical bond rather than simple physical mixture. The apparent rate constants  $k$  were 0.0418, 0.1052, 0.1512 and 0.1299 min<sup>-1</sup> for TCN-1, TCN-4, TCN-6 and TCN-8 catalysts, while the apparent rate constant  $k$  of the self-doped  $Ta_2O_5$  and  $g-C_3N_4$  were only 0.0005328 and 0.0127 min<sup>-1</sup>, which further confirmed the important role of the Ta—O—C chemical bond for the separation of the photo-induced electron and hole pairs, as depicted in Fig. 10(b). A reported apparent rate constant  $k$  of  $g-C_3N_4$ -ZnO composite for photodegradation of methyl orange was 0.0360 min<sup>-1</sup>, and another reported maximum apparent rate constant of  $GdVO_4/g-C_3N_4$  photocatalyst for RhB photodegradation was only 0.0434 min<sup>-1</sup>, much lower than that of TCN photocatalyst [63,64], which indicated TCN photocatalyst was an efficient photocatalyst for RhB degradation under visible light irradiation. As shown in Fig. 10(c), three recycling runs clearly revealed the good photochemical stability of TCN-6 catalyst for photocatalytic RhB degradation, and all the degradation yields were more than 96.76% (Fig. 10(d)). Based on the above analysis, TCN photocatalyst could be as a promising visible light photocatalyst for pollutant removal.

In order to investigate the roles of the hydroxyl radicals and holes in the RhB oxidation under visible light irradiation, the trapping experiments of TCN-6 catalyst by adding different sacrificial agents were conducted. As reported in literatures [65–67], ammonium oxalate and isopropanol could be used as the hole scavenger and  $\bullet OH$  quencher in the organic dyes degradation process, respectively. As shown in Fig. 11, almost all the RhB could be



**Fig. 11.** The active species trapping experiment of TCN-6 catalyst.

removed in about 20 min without adding any hole scavenger and  $\bullet OH$  quencher, also consistent with the above RhB degradation test. However, when ammonium oxalate was added into the RhB solution, the degradation rate of RhB was greatly suppressed, while it was barely affected in presence of isopropanol, which strongly indicated that RhB degradation with TCN catalyst could be mainly attributed to direct hole oxidation [33,66]. And holes were the main active species in the RhB degradation for TCN catalyst under visible light irradiation. The degradation reaction in this experiment seemed much like  $g-C_3N_4/TiO_2$  [68] in RhB degradation and could be described as follows,



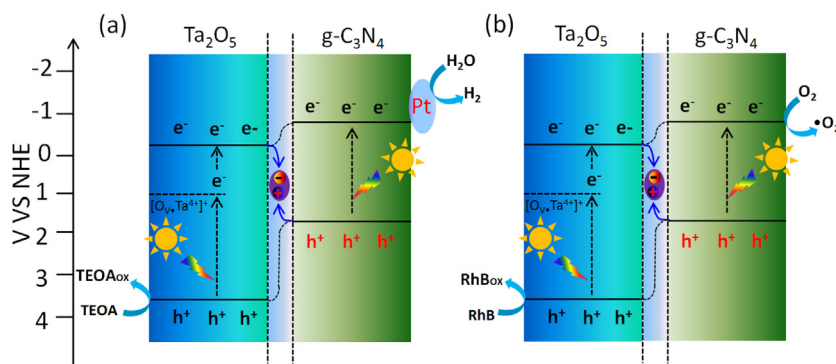


**Fig. 12.** Proposed direct Z-scheme mechanisms of TCN catalyst for (a) hydrogen production and (b) RhB degradation.

Based on the above analyses, possible direct Z-scheme mechanisms of TCN catalyst for hydrogen production and RhB degradation were proposed in Fig. 12.  $Ta^{4+}$  species was produced as well as the oxygen vacancy generation [47], and the oxygen vacancy ( $Ta^{4+}$  species) could have visible light response of the wide bandgap  $Ta_2O_5$  with a hydrogen production rate of  $7.98 \mu\text{mol g}^{-1} \text{h}^{-1}$ , showing its great advantage to compare with that of the commercial  $Ta_2O_5$ . In this experiment, the highly enhanced photocatalytic activities of TCN catalyst could be ascribed to the formation  $Ta^{4+}$  species and the Ta–O–C chemical bond, which highly promoted the charge separation for hydrogen production and RhB degradation. The conduction band of  $g\text{-}C_3N_4$  ( $-0.90 \text{ eV}$ ) was more negative compared with that of  $Ta_2O_5$  ( $-0.17 \text{ eV}$ ) [69] and  $H^+/\text{H}_2(0 \text{ eV})$ . And the reduction potential of  $O_2/\text{O}_2^-$  was  $-0.33 \text{ eV}$  [70], more negative than the conduction band of  $Ta_2O_5$  but positive than that of  $g\text{-}C_3N_4$ . And thus, the electrons of conduction band of  $g\text{-}C_3N_4$  had stronger reducibility than that of  $Ta_2O_5$ , and could react with dissolved  $O_2$  to form  $\text{O}_2^-$  or  $\text{H}_2O$  for hydrogen production, but the electrons of conduction band of  $Ta_2O_5$  did not because of the weaker reducibility [71]. And the photo-induced electrons of the conduction band of  $g\text{-}C_3N_4$  were likely to transfer to reaction active site for the reduction of  $\text{H}_2O$  or  $O_2$  dissolved in RhB solution to generate  $H_2$  or  $\text{O}_2^-$  species, while the electrons from the valence band of the  $Ta^{4+}$  doped  $Ta_2O_5$  leaped into  $Ta^{4+}$  defect energy level under visible light irradiation and then transferred to the conduction band of  $Ta_2O_5$  to react with the holes from the valence band of  $g\text{-}C_3N_4$  at the interface defect sites, as illustrated in Fig. 11. The holes of the valance band of  $Ta_2O_5$  were removed by TEOA oxidation or RhB degradation, which was also supported by the active species trapping experiment of TCN-6 catalyst. It was the formation of Ta–O–C chemical bond and  $Ta^{4+}$  defect energy level that effectively promoted charge separation between the self-doped  $Ta_2O_5$  and cotton-like  $g\text{-}C_3N_4$ , and highly enhanced the photocatalytic activity of TCN catalysts for hydrogen evolution and RhB degradation.

#### 4. Conclusions

We successfully prepared a novel  $Ta^{4+}$  self-doped  $Ta_2O_5$  quantum dots and the self-doped  $Ta_2O_5$  quantum dots modified cotton-like  $g\text{-}C_3N_4$  nanosheet by vapor hydrolysis reaction and calcining treatment for the first time. The as-prepared self-doped  $Ta_2O_5$  showed excellent visible light response from 400 nm to 800 nm and the amazing visible light photocatalytic activity for hydrogen production, mainly because of the formation of  $Ta^{4+}$  defect energy level in the self-doped  $Ta_2O_5$ . Besides, TCN photocatalyst displayed highly enhanced photocatalytic activities for hydrogen production and RhB degradation under visible light irradiation ( $\lambda > 420 \text{ nm}$ ), indicating the higher charge separation efficiency in comparison to those of the self-doped  $Ta_2O_5$  and

cotton-like  $g\text{-}C_3N_4$ . And it was the strong synergistic interactions of Ta–O–C chemical bond and  $Ta^{4+}$  defect energy level between the self-doped  $Ta_2O_5$  and cotton-like  $g\text{-}C_3N_4$  that highly enhanced the photocatalytic activity of TCN catalyst.

#### Acknowledgments

The authors would like to thank the partial financial support from the National Natural Science Foundation of China under grant no.51272052 and 50902040, the Heilongjiang Province Science Foundation for Young Scholar (QC2010065).

#### Appendix A. Supplementary data

Supplementary data associated with this article can be found, in the online version, at <http://dx.doi.org/10.1016/j.apcatb.2016.12.040>.

The SEM and high magnification TEM images of the as-prepared TCN-6 catalyst are shown in Fig. S1, and some recent studies on  $g\text{-}C_3N_4$ -based photocatalysts for hydrogen production and RhB degradation are shown in Table S1 and S2, which could be found in the online version.

#### References

- [1] A. Fujishima, K. Honda, *Nature* 238 (1972) 37–38.
- [2] X. Chen, S. Shen, L. Guo, S.S. Mao, *Chem. Rev.* 110 (2010) 6503–6570.
- [3] K. Maeda, K. Teramura, D.L. Lu, T. Takata, N. Saito, Y. Inoue, K. Domen, *Nature* 440 (2006), 295–295.
- [4] J.L. Gong, R. Luque, *Chem. Soc. Rev.* 43 (2014) 7466–7468.
- [5] A. Kudo, Y. Misaki, *Chem. Soc. Rev.* 38 (2009) 253–278.
- [6] P. Zhang, T. Wang, J. Gong, *Adv. Mater.* 27 (2015) 5328–5342.
- [7] S.G. Kumar, L.G. Devi, *J. Phys. Chem. A* 115 (2011) 13211–13241.
- [8] R. Asahi, T. Morikawa, H. Irie, T. Ohwaki, *Chem. Rev.* 114 (2014) 9824–9852.
- [9] C. Wang, D. Astruc, *Chem. Soc. Rev.* 43 (2014) 7188–7216.
- [10] L. Dai, Y. Xue, L. Qu, H.-J. Choi, J.-B. Baek, *Chem. Rev.* 115 (2015) 4823–4892.
- [11] Y. Luo, X. Liu, X. Tang, Y. Luo, Q. Zeng, X. Deng, S. Ding, Y. Sun, *J. Mater. Chem. A* 2 (2014) 14927–14939.
- [12] C. Zhou, L. Shang, H. Yu, T. Bian, L.-Z. Wu, C.-H. Tung, T. Zhang, *Catal. Today* 225 (2014) 158–163.
- [13] L. Xu, W. Shi, J. Guan, *Catal. Commun.* 25 (2012) 54–58.
- [14] J. Wang, J. Huang, H. Xie, A. Qu, *Int. J. Hydrogen Energy* 39 (2014) 6354–6363.
- [15] J. Liu, Y. Liu, N. Liu, Y. Han, X. Zhang, H. Huang, Y. Lifshitz, S.-T. Lee, J. Zhong, Z. Kang, *Science* 347 (2015) 970–974.
- [16] J. Zhang, X. Chen, K. Takanabe, K. Maeda, K. Domen, J.D. Epping, X. Fu, M. Antonietti, X. Wang, *Angew. Chem. Int. Ed.* 49 (2010) 441–444.
- [17] M. Zhang, W.J. Jiang, D. Liu, J. Wang, Y.F. Liu, Y.Y. Zhu, Y.F. Zhu, *Appl. Catal. B-Environ.* 183 (2016) 263–268.
- [18] J. Lin, Z. Pan, X. Wang, A.C.S. Sustain. Chem. Eng. 2 (2014) 353–358.
- [19] F. Dong, M. Ou, Y. Jiang, S. Guo, Z. Wu, *Ind. Eng. Chem. Res.* 53 (2014) 2318–2330.
- [20] A.B. Jorge, D.J. Martin, M.T.S. Dhanoa, A.S. Rahman, N. Makwana, J. Tang, A. Sella, F. Cora, S. Firth, J.A. Darr, P.F. McMillan, *J. Phys. Chem. C* 117 (2013) 7178–7185.
- [21] S. Chu, Y. Wang, Y. Guo, J. Feng, C. Wang, W. Luo, X. Fan, Z. Zou, *ACS Catal.* 3 (2013) 912–919.

[22] W.J. Ong, L.L. Tan, Y.H. Ng, S.T. Yong, S.P. Chai, *Chem. Rev.* 116 (2016) 7159–7329.

[23] X. Wang, K. Maeda, A. Thomas, K. Takanabe, G. Xin, J.M. Carlsson, K. Domen, M. Antonietti, *Nature Mater.* 8 (2009) 76–80.

[24] J. Zhang, M. Zhang, R.-Q. Sun, X. Wang, *Angew. Chem. Int. Ed.* 51 (2012) 10145–10149.

[25] Z.A. Lan, G.G. Zhang, X.C. Wang, *Appl. Catal. B-Environ.* 192 (2016) 116–125.

[26] J. Xue, S. Ma, Y. Zhou, Z. Zhang, M. He, *Acs Appl. Mater. Inter.* 7 (2015) 9630–9637.

[27] N. Tian, H. Huang, C. Liu, F. Dong, T. Zhang, X. Du, S. Yu, Y. Zhang, *J. Mater. Chem. A* 3 (2015) 17120–17129.

[28] W.J. Ong, L.K. Putri, L.L. Tan, S.P. Chai, S.T. Yong, *Appl. Catal. B-Environ.* 180 (2016) 530–543.

[29] J. Liu, S. Wen, Y. Hou, F. Zuo, G.J.O. Beran, P. Feng, *Angew. Chem. Int. Ed.* 52 (2013) 3241–3245.

[30] X. Dong, F. Cheng, *J. Mater. Chem. A* 3 (2015) 23642–23652.

[31] S.C. Yan, Z.S. Li, Z.G. Zou, *Langmuir* 25 (2009) 10397–10401.

[32] F. Dong, Z. Zhao, T. Xiong, Z. Ni, W. Zhang, Y. Sun, W.-K. Ho, *ACS Appl. Mater. Inter. Interfaces* 5 (2013) (1401) 11392–11401.

[33] N. Tian, H. Huang, Y. He, Y. Guo, T. Zhang, Y. Zhang, *Dalton Trans.* 44 (2015) 4297–4307.

[34] W.-J. Ong, L.-L. Tan, S.-P. Chai, S.-T. Yong, A.R. Mohamed, *Nano Energy* 13 (2015) 757–770.

[35] X. Wu, S. Yin, B. Liu, M. Kobayashi, M. Kakihana, T. Sato, *J. Mater. Chem. A* 2 (2014) 20832–20840.

[36] X. Wu, S. Yin, Q. Dong, T. Sato, *Phys. Chem. Chem. Phys.* 15 (2013) 20633–20640.

[37] M. Xu, L. Han, S. Dong, *Acs Appl. Mater. Interfaces* 5 (2013) 12533–12540.

[38] H. Yu, Y. Zhao, C. Zhou, L. Shang, Y. Peng, Y. Cao, L.-Z. Wu, C.-H. Tung, T. Zhang, *J. Mater. Chem. A* 2 (2014) 3344–3351.

[39] Y.J. Wang, R. Shi, J. Lin, Y.F. Zhu, *Energ. Environ. Sci.* 4 (2011) 2922–2929.

[40] R.V. Goncalves, R. Wojcieszak, P.M. Uberman, S.R. Teixeira, L.M. Rossi, *Phys. Chem. Chem. Phys.* 16 (2014) 5755–5762.

[41] J.Y. Zhang, B. Lim, I.W. Boyd, *Thin Solid Films* 336 (1998) 340–343.

[42] J.Y. Zhang, B. Lim, I.W. Boyd, *Appl. Surf. Sci.* 154 (2000) 382–386.

[43] X. She, H. Xu, H. Wang, J. Xia, Y. Song, J. Yan, Y. Xu, Q. Zhang, D. Du, H. Li, *T. Dalton.* (2015) 7021–7031.

[44] B. Neumann, P. Bogdanoff, H. Tributsch, S. Sakthivel, H. Kisch, *J. Phys. Chem. B* 109 (2005) 16579–16586.

[45] M. Lu, Z. Pei, S. Weng, W. Feng, Z. Fang, Z. Zheng, M. Huang, P. Liu, *Phys. Chem. Chem. Phys.* 16 (2014) 21280–21288.

[46] J. Lv, T. Kako, Z. Li, Z. Zou, J. Ye, *J. Phys. Chem. C* 114 (2010) 6157–6162.

[47] M. Xing, W. Fang, M. Nasir, Y. Ma, J. Zhang, M. Anpo, *J. Catal.* 297 (2013) 236–243.

[48] Y. Zhou, C. Chen, N. Wang, Y. Li, H. Ding, *J. Phys. Chem. C* 120 (2016) 6116–6124.

[49] H. Wang, X.Z. Yuan, H. Wang, X.H. Chen, Z.B. Wu, L.B. Jiang, W.P. Xiong, G.M. Zeng, *Appl. Catal. B-Environ.* 193 (2016) 36–46.

[50] Y. Cong, X. Li, Y. Qin, Z. Dong, G. Yuan, Z. Cui, X. Lai, *Appl. catal. B-Environ.* 107 (2011) 128–134.

[51] H. Shi, G. Chen, C. Zhang, Z. Zou, *ACS Catal.* 4 (2014) 3637–3643.

[52] W.J. Chun, A. Ishikawa, H. Fujisawa, T. Takata, J.N. Kondo, M. Hara, M. Kawai, Y. Matsumoto, K. Domen, *J. Phys. Chem. B* 107 (2003) 1798–1803.

[53] M. Xing, J. Zhang, F. Chen, B. Tian, *Chem. Commun.* 47 (2011) 4947–4949.

[54] E. Lira, S. Wendt, P. Huo, J.O. Hansen, R. Streber, S. Porsgaard, Y. Wei, R. Bechstein, E. Laegsgaard, F. Besenbacher, *J. Am. Chem. Soc.* 133 (2011) 6529–6532.

[55] C. Han, Y. Wang, Y. Lei, B. Wang, N. Wu, Q. Shi, Q. Li, *Nano Res.* 8 (2015) 1199–1209.

[56] K. Li, S. Gao, Q. Wang, H. Xu, Z. Wang, B. Huang, Y. Dai, J. Lu, *Acs Appl. Mater. Inter.* 7 (2015) 9023–9030.

[57] H.Q. Li, Y.X. Liu, Y.M. Cui, W.B. Zhang, C. Fu, X.C. Wang, *Appl. Catal. B-Environ.* 183 (2016) 426–432.

[58] X.J. Bai, R.L. Zong, C.X. Li, D. Liu, Y.F. Liu, Y.F. Zhu, *Appl. Catal. B-Environ.* 147 (2014) 82–91.

[59] S.L. Ma, S.H. Zhan, Y.N. Jia, Q. Shi, Q.X. Zhou, *Appl. Catal. B-Environ.* 186 (2016) 77–87.

[60] C.D. Lv, G. Chen, J.X. Sun, Y.S. Zhou, S. Fan, C.M. Zhang, *Appl. Catal. B-Environ.* 179 (2015) 54–60.

[61] M. Zhang, W.Q. Yao, Y.H. Lv, X.J. Bai, Y.F. Liu, W.J. Jiang, Y.F. Zhu, *J. Mater. Chem. A* 2 (2014) 11432–11438.

[62] P. Niu, L. Zhang, G. Liu, H.-M. Cheng, *Adv. Funct. Mater.* 22 (2012) 4763–4770.

[63] J.-X. Sun, Y.-P. Yuan, L.-G. Qiu, X. Jiang, A.-J. Xie, Y.-H. Shen, J.-F. Zhu, *Dalton Trans.* 41 (2012) 6756–6763.

[64] Y. He, J. Cai, T. Li, Y. Wu, H. Lin, L. Zhao, M. Luo, *Chem. Eng. J.* 215 (2013) 721–730.

[65] J. Wu, J. Wang, H. Li, Y. Du, X. Jia, B. Liu, *CrystEngComm* 16 (2014) 9675–9684.

[66] S. Chen, Y. Hu, S. Meng, X. Fu, *Appl. Catal. B-Environ.* 150 (2014) 564–573.

[67] J. Zhuang, W. Dai, Q. Tian, Z. Li, L. Xie, J. Wang, P. Liu, X. Shi, D. Wang, *Langmuir* 26 (2010) 9686–9694.

[68] R. Hao, G. Wang, H. Tang, L. Sun, C. Xu, D. Han, *Appl. Catal. B-Environ.* 187 (2016) 47–58.

[69] K. Maeda, K. Domen, *J. Phys. Chem. Lett.* 1 (2010) 2655–2661.

[70] Y.C. Deng, L. Tang, G.M. Zeng, J.J. Wang, Y.Y. Zhou, J.J. Wang, J. Tang, Y. Liu, B. Peng, F. Chen, *J. Mol. Catal. A: Chem.* 421 (2016) 209–221.

[71] R.Q. Ye, H.B. Fang, Y.Z. Zheng, N. Li, Y. Wang, X. Tao, *Acs Appl. Mater. Inter.* 8 (2016) 13879–13889.